ARTICLE IN PRESS

Available online at www.sciencedirect.com

ScienceDirect

ELSEVIER

Tribology International ▮ (▮▮▮▮) ▮▮▮–▮▮▮

TRIBOLOGY INTERNATIONAL

www.elsevier.com/locate/triboint

TiC_xO_y thin films for decorative applications: Tribocorrosion mechanisms and synergism

M.T. Mathew[a,*], E. Ariza[a], L.A. Rocha[a,b], A.C. Fernandes[c], F. Vaz[c]

[a]*Research Centre on Interfaces and Surfaces Performance, Azurém, 4800-058 Guimarães, Portugal*
[b]*Dept. Eng. Mecânica, Universidade do Minho, Azurém, 4800-058 Guimarães, Portugal*
[c]*Dept. Física, Universidade do Minho, Azurém, 4800-058 Guimarães, Portugal*

Received 27 February 2007; received in revised form 7 November 2007; accepted 12 November 2007

Abstract

Recently, tribocorrosion is widely accepted as an interdisciplinary area of research and such studies on various materials are gaining more attention by scientists and engineers due to its practical and economical significances in a wide range of applications. The main objective of the present work were to investigate the tribocorrosion behaviour of single layered titanium oxycarbide, TiC_xO_y, thin films on a reciprocating sliding tribometer, and in the presence of artificial sweat solution at room temperature, by considering the practical usage of such films as a decorative coating on various components.

The films were produced by DC reactive magnetron sputtering, using C pellets incrusted in the Ti target erosion area. A gas atmosphere composed of Ar and O_2 was used. The Ar flow was kept constant, and the oxygen gas flow varied from 0 to 10 sccm. During the wear tests both the open circuit potential and the corrosion current were monitored. Also, electrochemical impedance spectroscopy (EIS) tests were performed before and after sliding process. The modifications on the "native" coating microstructure and/or chemical composition induced by the variation of the deposition parameters were also evaluated and correlated with the wear–corrosion mechanisms occurring in each system.

The corrosion studies, including EIS measurements, exhibited the high corrosion resistance of the TiC_xO_y films, which is clear from the unchanged/constant values of the polarization resistance, before and after the sliding process, at the evaluated potential. The effects of hardness, thickness and structure of the films on their tribocorrosion performance, as a function of oxygen fraction, were studied and an attempt was made to classify them. Two of the eight films ($f_O = 0.55$ and 0.79), considered in the test, demonstrated better tribocorrosion resistance than others. Further, individual and synergistic effects of wear and corrosion on total wear loss were estimated and correlated with tribocorrosion mechanisms.

Keywords: Tribocorrosion; Wear mechanisms; Wear debris; Wear–corrosion volume; Synergistic effect

1. Introduction

In recent years, the studies on the processing, development and performance of thin films for decorative applications are gaining more and more importance in scientific research as well as in industrial environments [1–3]. The large usage of tiny components for a wide range of applications, such as mobile phones, mobile disks, etc., has significantly increased in the daily life of human beings. More than just protecting the surface, these coated objects are required to be attractive and eye catching, but above all to guaranty the durability and consistent surface characteristics. In this particular point, corrosion and wear of the coating materials represents a major concern for manufactures.

Since the 1990s, physical vapour deposition (PVD) coatings have been established as one of the highest quality finish technologies for sanitary and door hardware [1]. It acts as an alternative to traditional electroplating because of environmental reasons (it is recognized as being pollution free) and several other characteristics, such as

*Corresponding author.
E-mail address: mathew@dem.uminho.pt (M.T. Mathew).

0301-679X/$ - see front matter © 2007 Elsevier Ltd. All rights reserved.
doi:10.1016/j.triboint.2007.11.011

Nomenclature

M	atomic mass
C_C	carbon fraction
R_{ct}	charge transfer resistance at the interface
CPE	constant phase element
i_{corr}	corrosion current (A)
E_{corr}	corrosion potential (mV)
ε_0	dielectric constant in vacuum
ε	dielectric constant of the coating
C_{dl}	double layer capacitance
EIS	electrochemical spectroscopy impedance
R_e	electrolyte resistance
A	exposed area of the film (mm^2)
T	exposure time (s)
fcc	face-centered cubic
F	Faraday's constant ($96\,500\,C\,mol^{-1}$)
C_f	film capacitance
R_{pf}	film polarization resistance
hcp	hexagonal close-packed
$\|Z\|$	impedance modulus
f_O	notations of the films considered in the current work ($f_O = C_O/(C_O + C_C)$)
Z	number of electrons involved in the corrosion process
OCP	open circuit potential (mV)
C_O	oxygen fraction
R_p	polarization resistance
SCE	standard calomel electrode
R_{ps}	substrate polarization resistance
Q	the charge passed through the contact
d	thickness of the film (μm)
I	total current (A)
K_{wc}	total wear–corrosion (mm^3)
K_c	wear loss due to corrosion (mm^3)
K_w	wear loss due to sliding wear (mm^3)

high hardness and wear resistance, no discoloration or tarnishing, high corrosion resistance and no attack of ultraviolet (UV) radiation [1,2]. Several target materials, such as zirconium, titanium, chromium, vanadium, titanium–aluminium alloys and niobium, among others, can be used for coating application. Further with a multi-target system, it is also possible to make compound coatings from more than one metal [3]. By introducing reactive gases like nitrogen, methane, oxygen, etc., metal–nitride, metal–carbide, metal–carbonitride and metal–oxycarbide films may also be produced with enhanced surface characteristics (mechanical, tribological, etc.) and larger range of colour combinations [2–9].

Recently, transition-metal carbides, such as TiC, are becoming very attractive in the field of decorative films due to their interesting combined mechanical and physical properties. These coating materials show high-hardness and high-melting point, excellent electrical and thermal conductivity, as well as high chemical and thermal stability [10,11]. Furthermore, the addition of nitrogen to these carbide films has been shown to reduce the inner stress, electrical resistivity and friction coefficients [12,13]. Hence, oxygen was also found to be a good candidate for the improvement of TiC films, due to its high reactivity with most of the metals and the variations that might be induced in the optical and mechanical characteristics of the materials, by the changes that it may cause in chemical bonding states (for a general description of oxygen influence in well-known thin film materials see [4,8]). Therefore TiC_xO_y films are expected to have a wide spread of property variations [12], including the changes in optical characteristics (such as colour), keeping their mechanical/tribological consistency.

In terms of everyday life usage, decorative/protective coatings are exposed to various environmental conditions such as human sweat and extraneous particles like dust. Simultaneously, they are exposed to mechanical conditions such as rubbing and holding with hands. This is an area where the so-called tribocorrosion experiments may play a decisive role in order to simulate the real conditions of everyday usage. Tribocorrosion is a new area in materials research, which deals with the simultaneously mechanical (wear/scratching) and chemical (corrosion) effects on the material degradation [14,15].

Taking this into account, the aim of the current work is to study the tribocorrosion behaviour of multifunctional titanium oxycarbide thin films, TiC_xO_y, prepared by reactive magnetron sputtering, in artificial sweat solution, trying to bring some insights for its possible usage as protective/decorative thin films. In order to scan the largest possible number of material's properties variations, different films were prepared by varying the oxygen flow rate, which allowed to study most of the different tribological mechanisms present and thus to understand the oxygen influence in material's behaviour. Initial experiments were carried out to study the corrosive behaviour of these films and tribocorrosion experiments were done on a reciprocating tribometer. An attempt has also been made to analyse different mechanisms involved in the tribocorrosion process. The knowledge of the tribocorrosion behaviour of such films definitely assists in producing better films with expected performance characteristics for several decorative components.

2. Experimental details

2.1. Film preparation

Reactive DC magnetron sputtering was used to deposit TiC_xO_y films, from a Ti target ($200 \times 100\,mm^2$), with 12 cylindrical C pellets (10 mm diameter each, occupying an average area of $1200\,mm^2$) incrusted in the target erosion

Please cite this article as: Mathew MT, et al. TiC_xO_y thin films for decorative applications: Tribocorrosion mechanisms and.... Tribiol Int (2008), doi:10.1016/j.triboint.2007.11.011

zone (referred hereafter as a Ti(C) target). Films were deposited on polished high-speed steel (AISI M2) and single crystal silicon wafers ((1 0 0) orientation). All substrates were previously ultrasonically cleaned and sputter etched for 15 min in an Ar atmosphere (pressure of 0.15 Pa). The films were prepared with the substrate holder positioned at 70 mm in all runs, applying a DC current density of 75 A m^{-2} to the Ti(C) target. The base pressure was 2×10^{-3} Pa, while the Ar pressure during deposition varied between 0.4 and 0.5 Pa (corresponding to an argon flow of 60 sccm). The oxygen gas flow varied from 0 to 10 sccm (corresponding to a partial pressure variation between 0 and 8.6×10^{-2} Pa). The substrates were grounded during depositions.

The chemical composition of the coatings was investigated with a Cameca SX-50 Electron Probe Micro Analysis (EPMA), operating at 15 keV as acceleration voltage. The elemental quantification was performed by comparing the peak intensity in the sample and in standards for each element, and applying a ZAF correction to the results. The oxygen fraction in each sample was determined by the ratio between the oxygen concentration and the sum of both oxygen and carbon concentrations: $f_O = C_O/(C_O + C_C) = X$. The films are labelled as $f_O = X$. A short summary of all prepared samples is given in Table 1. Ball cratering tests were used to measure the thickness of the films. Surface and cross-section morphological features of the films were studied by scanning electron microscopy (SEM) and atomic force microscopy (AFM), while surface defects were characterized by optical microscopy (OM). Film's hardness and Young's modulus were determined from the loading and unloading curves, carried out with an ultra-low load-depth sensing Berkovich nanoindenter from CSM Instruments (Switzerland). The maximum load used was 30 mN, with a loading time of 30 s, holding 30 s and unloading in 30 s, producing an average number of 15 indentations per sample. The testing procedure includes the correction of the experimental results for geometrical defects in the tip of the indenter, thermal drift of the equipment and uncertainty in the initial contact. As the substrate surface was prepared in a similar metallographic method, before film deposition, the anticipated effect of substrate surface conditions on the hardness measurements might be uniform.

2.2. Preliminary corrosion tests

Before starting the tribocorrosion tests, an individual analysis on the basic corrosion behaviour of the samples was done by using a specially made corrosion cell. Open circuit potential (OCP) was monitored for 600 s followed by potentiodynamic polarization tests, in both substrate and TiC_xO_y films, between −0.8 and +2.0 V at scan rate 2 mV s^{-1}. The instrument used was a PGP201 Potentiostat/galvanostat (Radiomater analytical, Denmark), controlled by the Voltamaster-1 software.

2.3. Tribocorrosion tests

A schematic diagram of the tribocorrosion experimental set-up is shown in Fig. 1. Reciprocating sliding test apparatus, (Plint TE-67/R) was supplied by Phenoix Tribology Ltd. (UK) (earlier it was known as Plint and partners (Ltd)). Tests were conducted with an alumina pin (with truncated cone geometry) sliding on a plate sample (TiC_xO_y film) at a fixed normal load of 5 N. The sliding stroke length was 6 mm with a frequency of 1 Hz and an exposed area of 0.95 cm^{-2}. At the beginning of each test, the pin head was polished to maintain a constant diameter of 1 mm, and also to achieve consistent contact conditions between pin and sample. The electrolyte, artificial sweat solution was prepared according to Table 2, with a pH of 4.49 ± 0.01. The solution is a simplified version of that formalized in the European Standard EN 1811:1998 [16], and was contained in an acrylic cell with a volume of approximately 20 ml. A standard calomel electrode (SCE) was used as the reference electrode and a platinum wire was used as a counter electrode. The sample, TiC_xO_y film, was connected to the working electrode.

Prior to all tribocorrosion experiments, the samples were cathodically polarized at −900 mV vs. SCE during 180 s for the purpose of cleaning. Further, and in order to stabilize the sample, a potential of −660 mV was applied during 600 s, and then maintained during all the tests. Then, electrochemical impedance spectroscopy (EIS) was performed in the frequency range of 100 kHz to 15.82 mHz, with an AC sine wave amplitude of 10 mV applied to the electrode, keeping the sample under potentiostatic control, i.e. −660 mV (E_{corr} of the steel). The alumina pin was

Table 1
Details of the TiC_xO_y films considered in the tests

Sample	Oxygen fraction (f_O)	Thickness (μm)	Ti (at.%)	C (at.%)	O (at.%)	Hardness (GPa)	Number of defects (mm^2)
$TiC_{0.28}O_{0.14}$	0.33	6.3 ± 0.7	70.3	19.8	9.9	3.2	–
$TiC_{0.32}O_{0.17}$	0.35	4.8 ± 0.3	67.1	21.5	11.4	6.8	–
$TiC_{0.36}O_{0.45}$	0.55	5.8 ± 0.2	55.2	20.0	24.8	10.0	415
$TiC_{0.37}O_{0.76}$	0.67	5.2 ± 0.2	46.9	17.4	35.7	14.8	171
$TiC_{0.40}O_{1.52}$	0.79	4.4 ± 0.1	34.3	13.8	51.9	17.0	197
$TiC_{0.14}O_{1.51}$	0.92	5.8 ± 0.2	37.8	5.3	56.9	13.6	–
$TiC_{0.07}O_{2.31}$	0.97	1.5 ± 0.4	29.6	1.9	68.5	9.2	99
TiO_2	1	1.2 ± 0.4	33.3	0	66.6	9.6	596

Please cite this article as: Mathew MT, et al. TiC_xO_y thin films for decorative applications: Tribocorrosion mechanisms and.... Tribiol Int (2008), doi:10.1016/j.triboint.2007.11.011

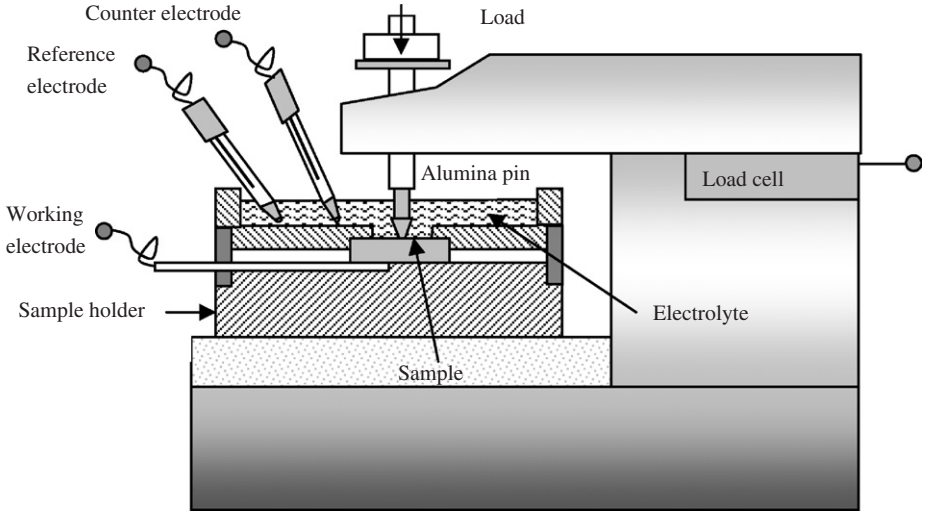

Fig. 1. Schematic diagram of reciprocating pin/ball tribometer coupled with electrochemical cell.

Table 2
Composition of artificial sweat solution [16]

Components	Composition
NaCl	7.5 g l^{-1}
KCl	1 g l^{-1}
CH_4N_2O (urea)	1 g l^{-1}
$C_3H_6O_3$ (lactic acid)	1 ml l^{-1}
NH_3 added to adjust the pH of 4.49	

brought in contact with the plate sample. The reciprocating sliding tests were conducted during 3600 s. An EIS test was performed at the end of the experiment, after stabilization of the sample. At the end of the test, pin and sample were ultrasonically cleaned by propanol and distilled water. Each experiment was repeated twice, and one set of the test ($f_O = 0.92$) was repeated 3 times to estimate the expected error (5–7%) in the tests. For EIS data simulation the Z-View software was used. The wear volume was determined by profilometry, using a Perthometer S5P surface measuring and recording instrument, by measuring the cross-sectional area and stroke length. The cross sectional area and depth of the wear profiles were measured with the help of AutoCAD 2006.

3. Results and discussion

3.1. Surface and morphological characterization

The worn surfaces were studied by using OM, SEM and AFM images. An AFM image obtained for the film with $f_O = 1$ (a TiO_2 film) is shown in Fig. 2(a). An AFM image of a corrosion pit formed on the surface of the film with $f_O = 0.97$ is also shown in Fig. 2(b). The micrographs obtained by OM (Figs. 2(c) and (d)) show the corroded surfaces of films with $f_O = 0.33$ and $f_O = 0.97$, illustrating the pitting process after the polarization test.

Representative SEM images of the worn surfaces are shown in Figs. 3(a)–(f). Fig. 3(a) shows the pin path and worn surface on the film with $f_O = 0.35$. It is worth to observe the presence of a special region, consisting of heavy plastic deformation, close to the boundary of the pin path (Fig. 3(b)). Fig. 3(c) shows the clear boundary of the worn surface of the film with $f_O = 0.67$. Worn surfaces of the films with $f_O = 0.33$, 0.92 and 1 are shown in Figs. 3(d), (e), and (f), respectively. They demonstrate the presence of four regimes on the worn surface, i.e., A, B, C and D, which will be discussed further in Section 3.8.

3.2. Initial corrosion tests

In Fig. 4, an overlap of the potentiodynamic polarization curves obtained for some representative TiC_xO_y films (films with $f_O = 0.33$, 0.97 and 1) is presented. The polarization curve of the M2 steel, used as substrate, is also plotted. The initial observation is that the films clearly show good corrosion resistance, compared to the substrate material. In fact, the results of potentiodynamic polarization tests, shown in Fig. 4, reveal that the corrosion resistance of the substrate is clearly improved by the deposition of the films. In all cases the corrosion current density of the films, i_{corr}, is below 1 μA cm^{-2}, which is significantly lower than that of the substrate ($i_{corr} = 3.47$ μA cm^{-2}). A pitting potential is observed in all films.

As stated above, the presence of pits after the polarization tests was examined by OM, AFM and SEM analysis and correlated with the pitting behaviour (see Figs. 2(c), (d) and 3(b)). The film with $f_O = 0.33$ shows the highest pitting potential, followed, in decreasing order, by the films with $f_O = 1$ and $f_O = 0.97$, indicating that a better pitting corrosion resistance is present in the films with the lowest oxygen fraction. These results indicate that, similar to what has been observed for the film's physical and mechanical properties [4,14,15,17], the composition of the samples and the consequent structural/morphological changes are also

Please cite this article as: Mathew MT, et al. TiC_xO_y thin films for decorative applications: Tribocorrosion mechanisms and.... Tribiol Int (2008), doi:10.1016/j.triboint.2007.11.011

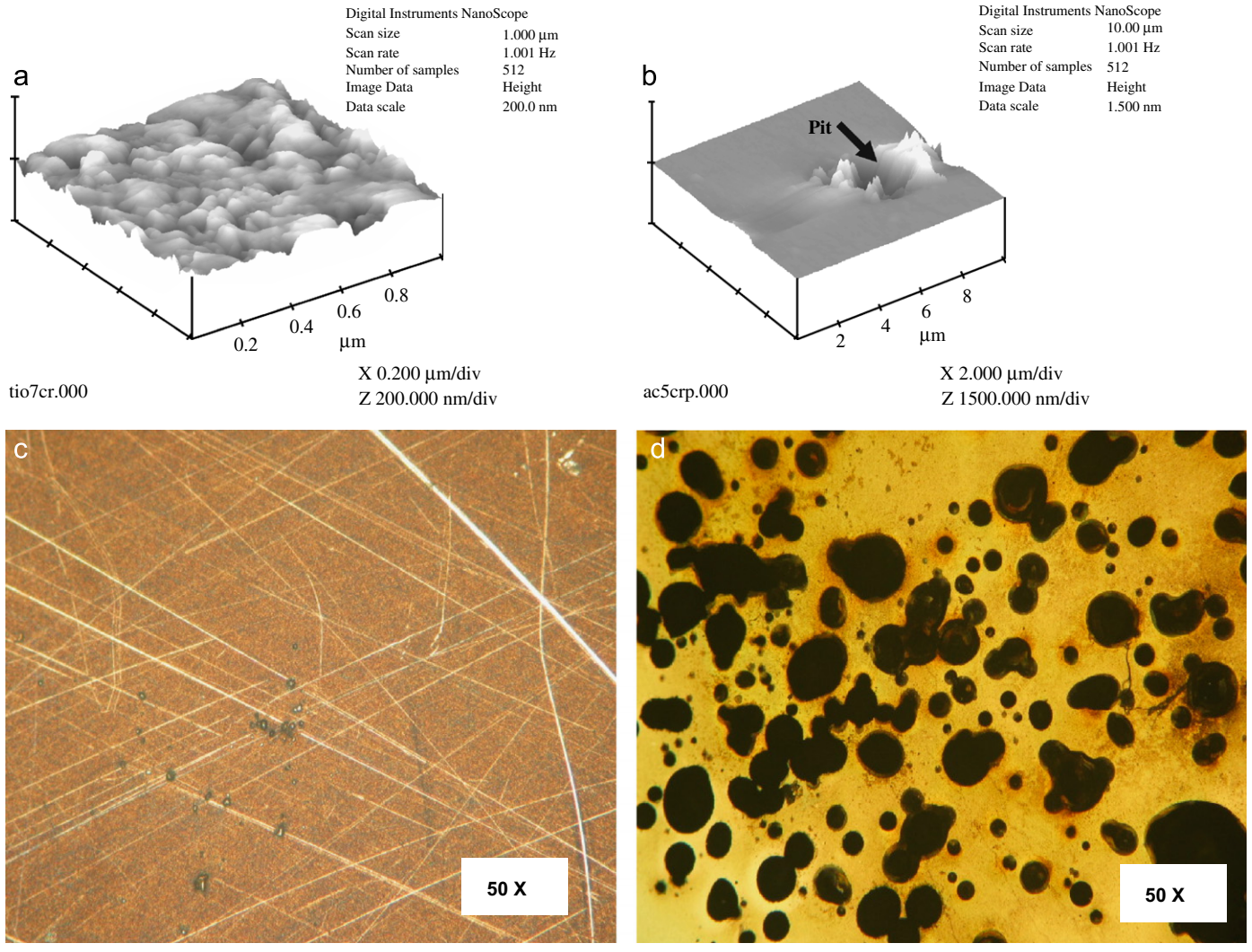

Fig. 2. Typical micrographs and AFM images of the films surfaces, after the test. (a) Plane surface of $f_O = 1$. (b) Worn surface of $f_O = 0.97$ showing a pit. (c) Micrograph of corroded surface of $f_O = 0.33$, showing the influence of pitting potential. (d) Micrograph of corroded surfaces of $f_O = 0.97$, showing the influence of pitting potential.

ruling their corrosion behaviour. In fact, in the $f_O = 0.33$ film, a small and almost imperceptible quantity of pits was observed after the polarization test (Fig. 2(c)), when compared to the $f_O = 0.97$ film (Fig. 2(d)). The amount of surface defects of the as-produced films might have some influence on the pitting initiation stage. In fact, as shown in Table 1, the sample with $f_O = 0.33$ shows almost no surface defects when observed by OM. However, the lowest pitting potential was observed in the film with $f_O = 0.97$, which presented a lower number of defects (99 deffects mm^{-2} in comparison with the 596 defects mm^{-2} for the film with $f_O = 1$). This result suggests that other parameters, related to the structure of the films, were affecting the corrosion behaviour. Also, no direct correlation between film thickness and corrosion behaviour (i_{corr} or pitting potential) could be established (see Table 1 and Fig. 4), which again reinforces the latter assumption.

Interestingly, films with $f_O = 0.97$ and $f_O = 1$ show two distinct passive regions. This phenomenon is not completely clarified, but it can be related to a preferential dissolution of anatase and rutile—TiO_2 phases in this kind of films. In fact, as described in a previous work [17], while the $f_O = 0.33$ film, presenting the lowest oxygen fraction, is basically constituted by a mixture of hexagonal close-packed (hcp) Ti and face-centered cubic (fcc) TiC(O) phase, these last two films ($f_O = 0.97$ and $f_O = 1$), with the highest oxygen fractions, are mainly characterized by the presence of a mixture of poorly crystallized TiO_2 rutile and anatase phases. Further explanations on the influence of structural variation on the observed behaviour are addressed in Section 3.9.

3.3. Tribocorrosion performance

The evolution of the current density and friction coefficient values during the tribocorrosion tests, for each film, was analysed. Fig. 5 shows representative curves of the observed trends: (a) for the film with $f_O = 0.55$ and

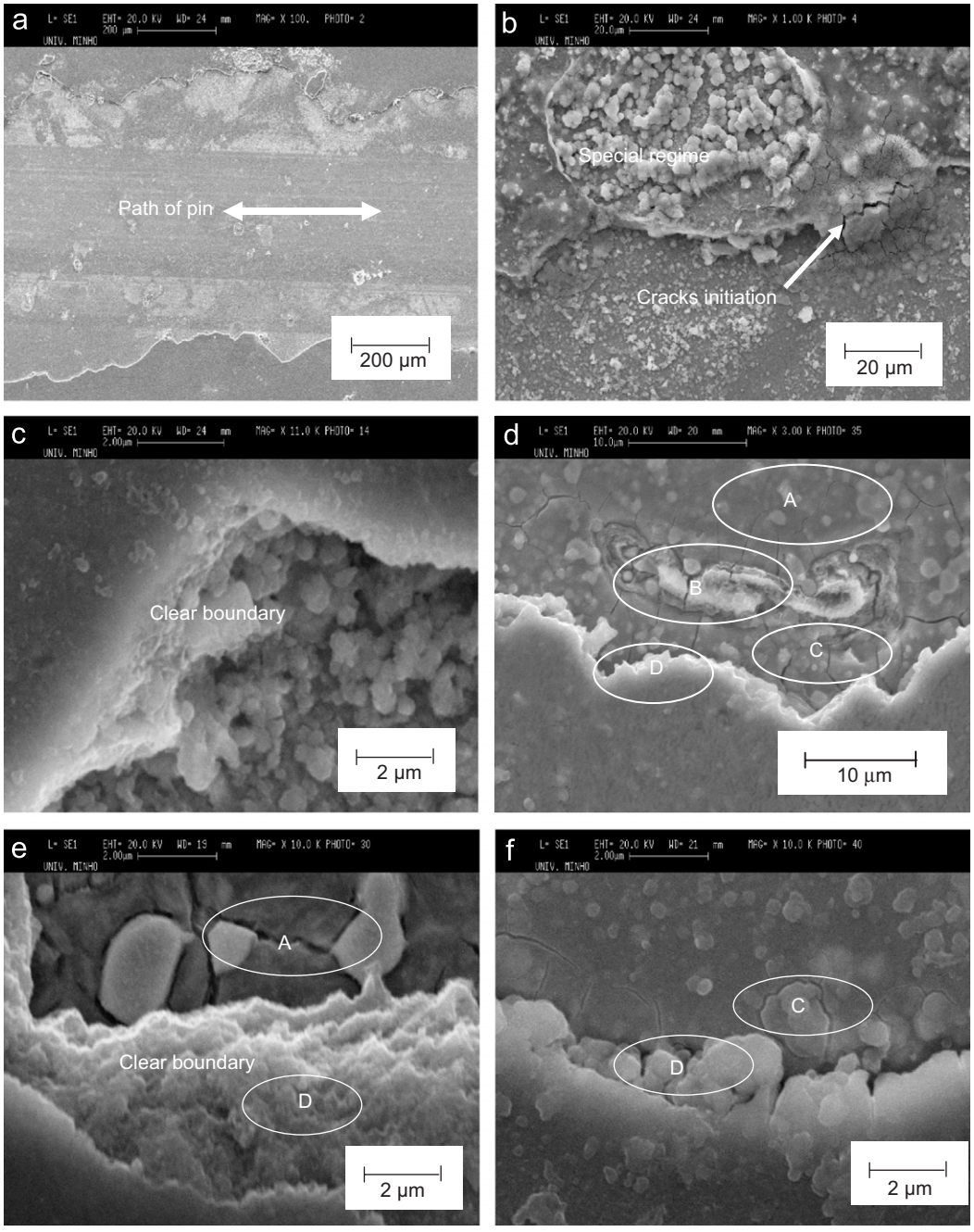

Fig. 3. SEM images of the worn surfaces. (a) Pin mark on the surface of $f_O = 0.35$. (b) Cracks and special regime formed on the worn surface. (c) Boundary of the wear path with high magnification ($f_O = 0.67$). (d) Crack and special regime on $f_O = 0.33$. (e) Clear boundary on $f_O = 0.92$. (f) Completely removed $f_O = 1$.

(b) for the film with $f_O = 0.79$. As it can be observed in the graph (Fig. 5(a)), the current density decreases with the increase in the sliding time. Accumulation of wear debris and corrosion product in contact zone can be the reason for the reduction in the current density during the sliding process.

Studies on tribocorrosion behaviour of Fe-1 Cr in acid and alkaline solutions reported that in a reciprocating sliding tribometer, the instantaneous current is a periodic function, depending on the pin motion, which moves at a constant speed during a forward stroke and then remains stationary for a few milliseconds before changing its direction [18]. It was observed that during the rest period, the current decreases due to repassivation, and then increases again when the pin starts to return. Pontiaux et al. [19] also suggested that the main concern in wear–corrosion studies on the current set-up is that the reciprocating pin motion creates non-steady electrochemical conditions at the contact zone. However, electrochemical interfacing techniques favour stationary conditions in/during the test. Hence the dynamic and transient condition at the contact zone might influence the obtained results.

Please cite this article as: Mathew MT, et al. TiC_xO_y thin films for decorative applications: Tribocorrosion mechanisms and.... Tribiol Int (2008), doi:10.1016/j.triboint.2007.11.011

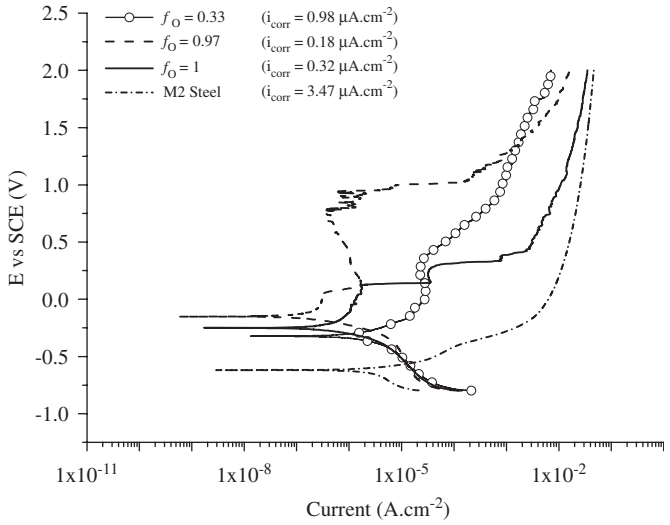

Fig. 4. Potentiodynamic polarization curves obtained for some representative TiC_xO_y films immersed in artificial sweat solution.

The friction coefficient values are also observed to be very sensitive to the sliding process. Generally, the values of friction coefficients remain stable after an initial running-in period. This is the case in the film with $f_O = 0.55$, (Fig. 5(a)). However, in some cases, there was a gradual increment in the values of friction coefficients after the first half of the test. As an example, the case of the film with $f_O = 0.79$ (Fig. 5(b)). The increase in the friction coefficient during sliding was also reported in earlier studies, and it is suggested that such behaviour may be due to the presence of corrosion products and wear debris formed during the sliding process [14]. Further, close observation on Figs. 5(a) and (b) (marked as A and B) shows that the increase in friction coefficient is accompanied by the decrease and/or fluctuations in corrosion current, which is ensuring the existence of such situation in the current study. However, additional analysis is required to gain more understanding on such interesting tribocorrosion phenomena and associated effects on the material degradation process.

3.4. Electrochemical impedance spectroscopy (EIS) analysis

In Fig. 6, results of EIS tests for some representative TiC_xO_y films ($f_O = 0.33$, 0.97 and 1) before and after sliding processes are presented. Fig. 6(a) shows the Bode Z plot (frequency vs. impedance modulus $|Z|$), while Fig. 6(b) presents the Bode phase plot (frequency vs. phase angle).

Results of EIS data simulations are presented in Fig. 7. In all cases it was assumed an electrochemical equivalent circuit composed by the electrolyte resistance (R_e) in series with one pair of elements in parallel. This pair of elements represents the dielectric properties of the film, and is composed of the film capacitance (C_f) and by the film polarization resistance (R_{pf}). An exception occurs with the film with $f_O = 1$ in which a second pair of elements was

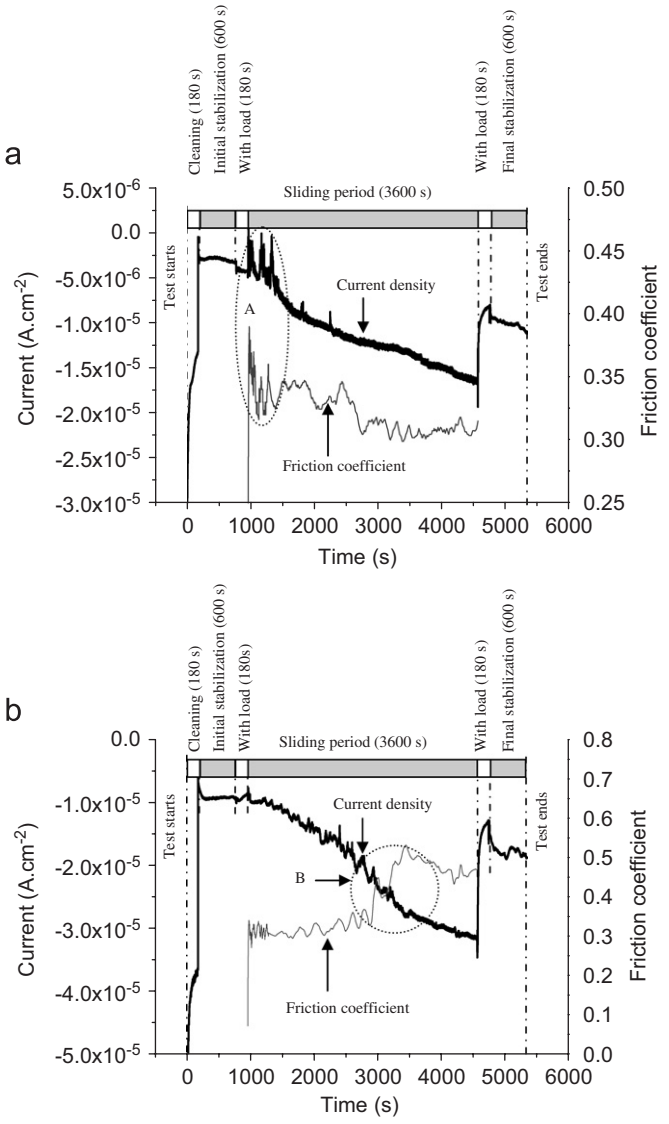

Fig. 5. Variation of corrosion current and friction coefficient values with sliding time for (a) $f_O = 0.55$ and (b) $f_O = 0.79$.

added in series with the first one. This last electrical pair is related to the processes occurring at the electrolyte/substrate interface and is composed of the same electric elements: the double layer capacitance (C_{dl}) and the charge transfer resistance at the interface (R_{ct}). In both equivalent circuits a constant phase element (CPE) was used to replace the pure one, which rarely occurs in a real process. A good agreement between the fitted and the experimental data was obtained.

Fig. 7(a) shows the evolution of the film thickness and of the polarization resistance (R_p) estimated before and after the sliding tests as a function of oxygen fraction (f_O). In the case of the film with $f_O = 1$, R_p was calculated by the sum of substrate polarization resistance (R_{ps}) and film polarization resistance (R_{pf}) as generally assumed as frequency tends to zero and assuming that $R_{ps} + R_{pf} \gg 0$ [20]. Additionally, Fig. 7(b) presents the evolution of the film thickness and the film capacitance (C_f) estimated before

Please cite this article as: Mathew MT, et al. TiC_xO_y thin films for decorative applications: Tribocorrosion mechanisms and.... Tribiol Int (2008), doi:10.1016/j.triboint.2007.11.011

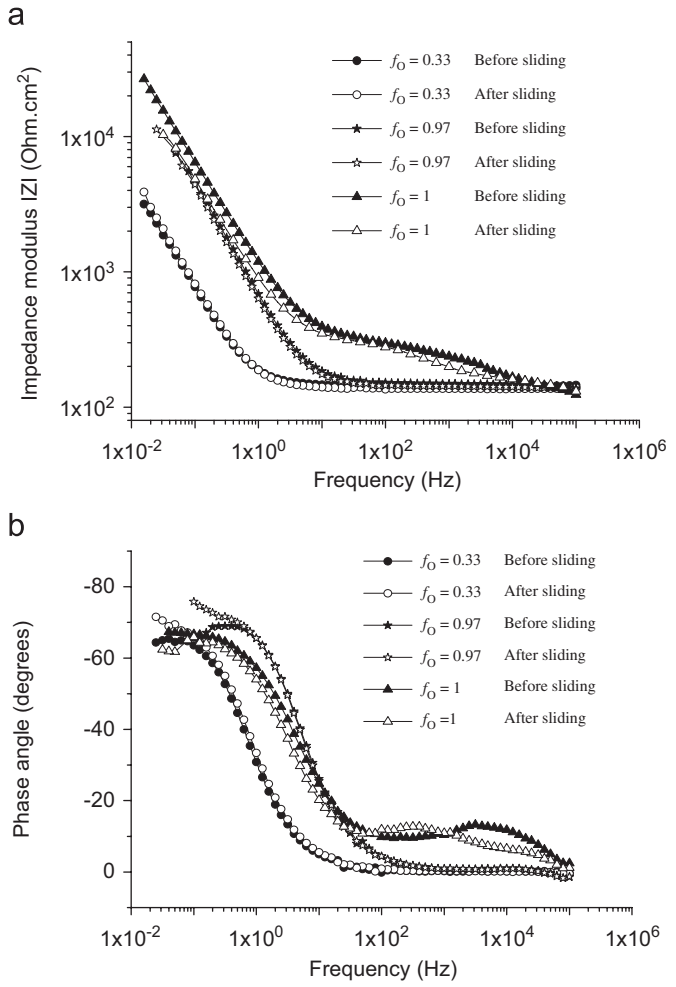

Fig. 6. EIS (electrochemical impedance spectroscopy) results obtained for some representative TiC_xO_y films ($f_O = 0.33$, 0.97 and 1) before and after sliding processes. (a) Bode Z plot (frequency vs. impedance modulus $|Z|$). (b) Bode phase plot (frequency vs. phase angle).

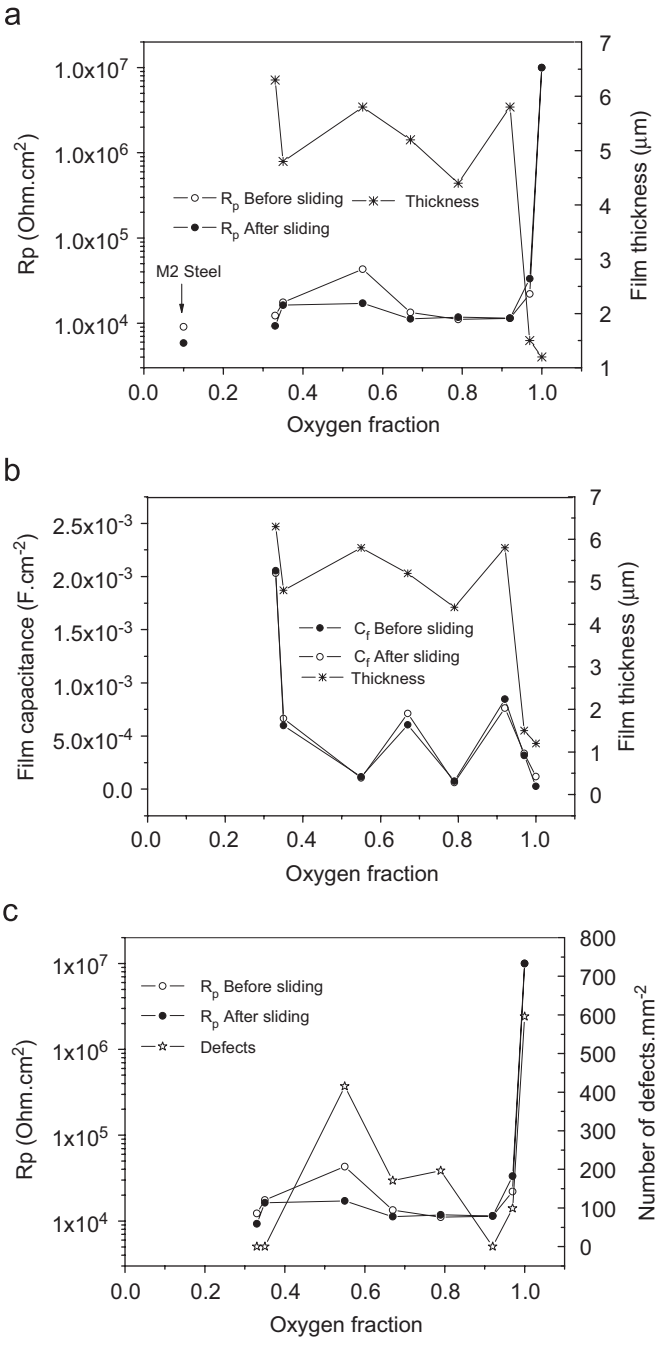

Fig. 7. Results of the EIS analysis. (a) Evolution of the polarization resistance (R_p) and film thickness with the oxygen fraction, before and after sliding time. (b) Evolution of the film capacitance and film thickness with the oxygen fraction, before and after sliding time. (c) Evolution of the polarization resistance and number of defects with the oxygen fraction, before and after sliding time.

and after sliding tests, as a function of f_O. Finally, Fig. 7(c) shows the evolution of the number of defects and R_p before and after the sliding process as a function of f_O.

As it can be observed in Fig. 6, EIS spectra, the electrochemical behaviour of the films is slightly altered after the sliding process, showing the good corrosion behaviour at the tested potential. An important characteristic to be mentioned is the presence of a clear second time constant in the case of the film with $f_O = 1$ (see Fig. 6(b)), which is probably related to the large number of defects present in this film (see Table 1). Nevertheless, this behaviour is quite similar for both $f_O = 1$ and $f_O = 0.97$, which are the films with the highest impedance (see Fig. 6(a)). This result shows that the films produced with higher oxygen fractions have better corrosion behaviour. However, it should be noted that the diverse pitting corrosive behaviour, see Section 3.2, also should be a factor in determining the best film. Again the different structural features revealed by these films (developing highly insulating oxide type structures in comparison to metallic hcp Ti and fcc-based Ti(O,C) in the others [17]), play a fundamental role for such behaviour.

After EIS data simulation, Fig. 7(a), an apparent general trend of an improvement of the polarization resistance with the increase in the oxygen fraction is detected. Results show, as already mentioned, R_p of the films at the evaluated potential (−660 mV), i.e., corrosion potential of the steel substrate, −600 mV vs. SCE, but a cathodic

potential regarding the films (see Fig. 4) has slightly changed after the sliding; only the film with $f_O = 0.55$ shows a clear decrease of the R_p after the sliding time. This suggests that at this potential the wear/corrosion process does not affect significantly the performance of the films, revealing their good corrosion behaviour. The high value of R_p obtained in the film with $f_O = 1$, showing the lowest thickness and very low R_{pf} value ($200\,\Omega\,cm^2$, as calculated by EIS data simulation), is mainly due to the higher R_{ct} revealed by the film. In fact, SEM analysis of the film shows the most compact structure at the film/substrate interface providing a higher R_{ct}, and consequently a higher R_p value. On the other hand, the lower R_{pf} value can be related to the high quantity of porosity existing in this film (see Table 1).

As mentioned above, the C_f and R_{pf} values are related to the dielectric properties of the films. Also, it is known that $C_f = \varepsilon\varepsilon_o A/d$, where ε is the dielectric constant of the coating, ε_0 is the dielectric constant in vacuum, A is the exposed area of the film and d is the thickness of the film. As it can be observed in Fig. 7(b), results suggest that the film thickness appears not to have a clear influence on the capacitance of the film but the main difference between the films can be due to their different physical properties [17], including the structure and the dielectric constants. In fact, films with higher oxygen fraction, especially that with $f_O = 1$, reveal the lowest C_f, which can be related to the comparatively low dielectric constant characteristic of the rutile and anatase phases of the TiO_2, when compared with the other more metallic-type films. In fact, high insulated properties, i.e., high electrical resistivity was measured in this film and others with similar characteristics (prepared with higher oxygen flows, and revealing oxide-type structures) [17]. Also, it is important to mention that the small changes observed in C_f after sliding (see Fig. 7(b)), show the good protective character and the low degradation suffered by the films after sliding tests.

Finally, it should be emphasize that in accordance with the electrochemical polarization results and EIS results showed that the corrosion properties do not have a clear dependence from the film thickness and/or the presence of defects as it can be observed in Figs. 7(a) and (c). These results support the idea that corrosion properties are primarily dependent on the structural properties of the films and further explanations are given in Section 3.9.

3.5. The variation in wear–corrosion volume loss as a function of oxygen fraction

The variation of total wear loss due to mechanical (wear) and chemical (corrosion) effects (which can be termed as K_{wc}, further explanations given in next section), for the various films that are considered in the test, is shown in Fig. 8(a). It is clear that the main trends in the variation of wear–corrosion volume loss with oxygen fraction can be distinguished within four zones. The films corresponding to low oxygen fractions (with a metallic-like Ti(C,O) fcc-type

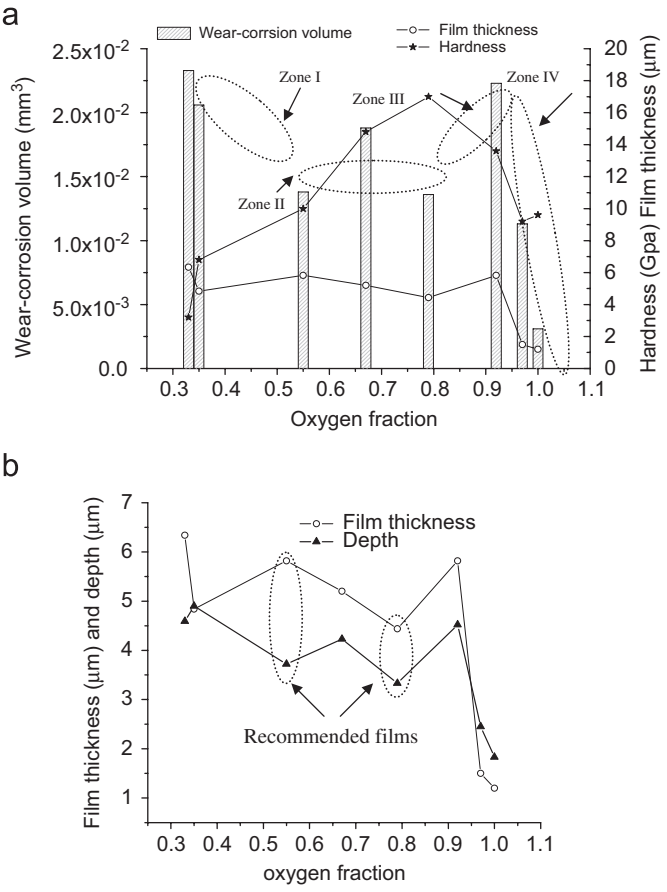

Fig. 8. Variation of wear–corrosion volume as a function of film thickness, hardness and depth of the wear profile. (a) Variation of wear–corrosion volume in relation to film thickness, hardness. (b) Variation of film thickness and depth of the wear profile/track.

structure and hcp Ti [17]) exhibit high wear volume loss and further demonstrate a reduction zone (zone I) within the range $0.3 < f_O < 0.5$ (Fig. 8(a)). Additionally, there is a stabilized zone II, for films with an oxygen fraction varying between 0.5 and 0.8, followed by an increasing zone III, corresponding to oxygen fractions of 0.8–0.9. For oxygen fractions above 0.9, a sudden reduction in wear volume loss is revealed, zone IV. It can be noted that the distribution of the above zones is matching with the structural variation of the films as a function of oxygen fraction [17] and more details are given in Section 3.9.

Furthermore, the graph also shows that the hardness and film thickness does not have much influence on wear volume loss, which is against what one would expect [21]. For instance, the film with maximum thickness, i.e., that with $f_O = 0.33$, shows higher wear volume and the film with minimum thickness, i.e., $f_O = 1$ shows the lowest wear volume loss. To explore further the results, the depth of the worn profile was estimated and compared with thickness (Fig. 8(b)), which will help to identify the film was removed completely or not, after the tribocorrosion test. It is obvious that most of the films are not removed completely. This shows that the current system (when we considered film and substrate as a integrated body) exhibit good

performance in contrast with other thin films, for instance decorative ZrO_xN_y films, which have been previously investigated in the group [14]. Further explanation on the effect of thickness is addressed in next Section 3.6.

3.6. Classification of the films based on tribocorrosion behaviour

In order to gather the general tribocorrosion behaviour of the films or rather film system from the current study, a methodology was adopted as illustrated below. As it was observed in the previous Section 3.5, the films can be easily classified into two sets, one set which is without any retention of the film after the tribocorrosion test and another set that retains film, as shown in the schematic diagram (Figs. 9(a) and (b)). The films with $f_O = 0.35$, 0.97 and 1 belong to the former set and the other five films correspond to the latter set. It is clear that in order to do such analyse on the performance of the films based on the thickness, it is necessary to have all the films in one category. However, in the present study the film thickness is also a variable. Moreover, it was observed that more than the thickness, structure of the films has a strong influence on the tribocorrosion behaviour. Hence, it is very difficult to classify or recommend the best films that are considered in the test.

In another perception, it is also very clear that the samples that retain film are really showing the performance of the film system against tribocorrosion. As it would be expected, the wear volume loss depends on the thickness, structure and hardness and other properties of the films. Hence, it can be concluded that there would be a critical thickness for the films, having better structure and other properties favourable to tribocorrosion resistance. However, it may be too early for such conclusion as in the current study was focused on the influence of oxygen fraction; the above parameters are also variables. In the next stage of work, in-depth study will definitely be considered in order to draw coherent understanding of tribocorrosion behaviour of individual films as a function of film thickness; hardness and structure (see Section 3.9). Hence, by acknowledging the limitation of the study and based on the current results on the wear volume loss, thickness of the film and depth of the wear profile (Fig. 8(b)), it is clear that the films with $f_O = 0.55$ and 0.79 show good performance compared to the others.

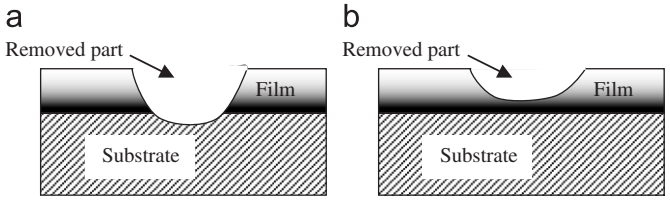

Fig. 9. Samples with two types of situations after the wear–corrosion (tribocorrosion) test. (a) Worn profile with retention of film. (b) Worn profile reaching to the substrate.

3.7. Analysis on synergistic effects of wear and corrosion

In tribocorrosion studies, it is useful to estimate the individual contribution of wear and corrosion to understand their synergistic or antagonistic effects on the total material removal. As observed in the last section (Section 3.6), five samples retain the films after one hour of sliding. Hence, those films are selected for the further analysis on the synergistic effects of wear and corrosion.

The total wear–corrosion volume loss may be explained by defining the following terms, using methodology developed by Yue and Shi [22], in the wear–corrosion analysis. If

$$K_{wc} = K_w + K_c, \tag{1}$$

where K_{wc} is the total wear–corrosion, K_w is the total wear loss due to sliding wear and K_c is due to corrosion.

The results of the various contributions to wear volume loss are given in Table 3 and Fig. 10. The volume loss due to the corrosion, K_c, is derived using Faraday's law, e.g.

$$K_c = Q/ZF, \tag{2}$$

$$K_c = MIt/ZF, \tag{3}$$

where Q is the charge passed, F is Faraday's constant (96 500 C mol^{-1}), Z is the number of electrons involved in the corrosion process (in the current study it was considered as 2), I is the total current, t the exposure time and M is the atomic mass of the material.

Table 3
Wear volume loss data by corrosion and wear

Films	K_c ($\times 10^{-5}$ mm^3)	K_{wc} ($\times 10^{-2}$ mm^3)	K_w ($\times 10^{-2}$ mm^3)	K_c/K_w ($\times 10^{-3}$)
$f_O = 0.33$	3.98	2.33	2.34	1.7
$f_O = 0.55$	5.01	1.38	1.38	3.6
$f_O = 0.67$	1.46	1.88	1.88	0.8
$f_O = 0.79$	3.99	1.36	1.36	2.9
$f_O = 0.92$	9.22	2.23	2.22	4.2

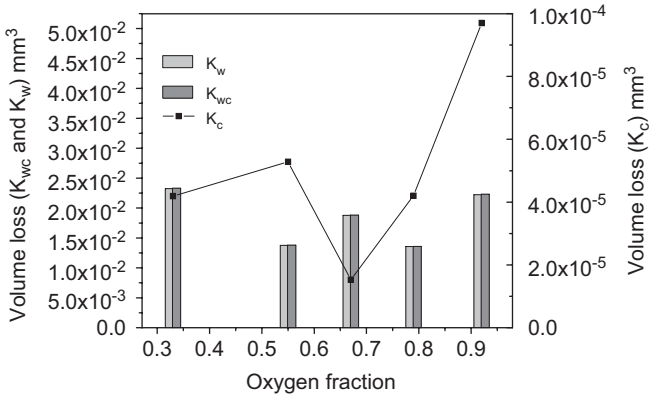

Fig. 10. Contribution of corrosion (K_c) and wear (K_w) to total wear volume loss (K_{wc}).

As stated above, in the current study, the tests were conducted at a potential of −660 mV vs. SCE, which correspond to a low corrosion rate (in cathodic region, see the polarization curves, Fig. 4). Hence, it is not surprising to observe that the K_c values are very small or rather negligible in comparison with K_w, which are almost equal to K_{wc} (Fig. 10). Generally, there is an increasing trend in the case of K_c, as oxygen fraction increases except for the film with $f_O = 0.67$. It can be speculated that such special behaviour of the films is the result of the influence of variation in film structure [17], as indicated in the earlier sections.

In order to understand the synergistic effects, K_c/K_w ratio was estimated, as shown in Table 3. As it is observed from the literature, Stack et al. [23–25] in their extensive studies on erosion–corrosion and wear–corrosion have established various regimes to identify the dominating mechanisms in the tribocorrosion process. The major criteria are listed below:

$$K_c/K_w \leqslant 0.1 \quad \text{(wear)}, \tag{4}$$

$$0.1 < K_c/K_w \leqslant 1 \quad \text{(wear} - \text{corrosion)}, \tag{5}$$

$$1 < K_c/K_w \leqslant 10 \quad \text{(corrosion} - \text{wear)}, \tag{6}$$

$$K_c/K_w \leqslant 10 \quad \text{(corrosion)}. \tag{7}$$

Hence, it is clear from Eq. (4) and Table 3 that the tribocorrosion process in the current study is entirely dominated by wear process or mechanisms. EIS analysis (Figs. 6 and 7) and SEM images of the worn surfaces (Figs. 3(b)–(f)) also supports this conclusion. The average values of K_c for the films with $f_O = 0.55$ and $f_O = 0.79$, are indicative of their good characteristics. Furthermore and in order to understand the clear influence of synergistic effects on the tribocorrosion process, the analyses are to be conducted by varying the mechanical parameters, such as load and sliding velocity, etc. [26]. There is also possibility of the tribofilm formation at the contact zone and which can protect the surface from corrosion, showing the additive effect of wear on corrosion. However, in the present study such analysis is beyond the scope.

3.8. Mechanisms of wear–corrosion process

In order to analyse the mechanisms involved in the tribocorrosion process, a schematic diagram of the contact zone is shown in Fig. 11. The top view of the contact zone during the tribocorrosion process shows the presence of four regions:

Region A: Pin path (severe wear).

Region B: Sides of the pin path, corrosion prone area, presence of wear debris (severe wear).

Region C: Corrosion prone area, collection of wear debris (low wear).

Region D: Corrosion prone area, in the boundary (low wear, cracks initiation).

It is well known that, in the case of a reciprocating sliding system, the material removal may be the result of several mechanisms, which are directly or indirectly involved in the process [22–28]. In the initial stage of the sliding, the main mechanisms that drive the material removal may be the ploughing and cutting process, which result from the strong action of the alumina pin, and high contact pressure by the applied load.

It was also reported by other studies that the mechanisms may also be dominated by three body situations by formation of wear debris and corrosion products, which remain in the tribological contact for a certain period before they are eliminated [28–33], as shown in Fig. 11. The presence of a third body in a tribological contact can have

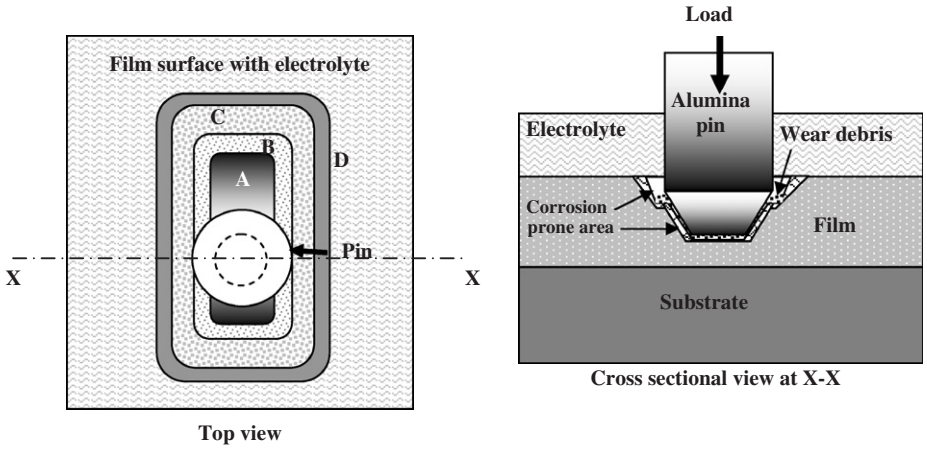

Four regions:
Region A: Pin path (severe wear)
Region B: Sides of the pin path, corrosion prone area, presence of wear debris (severe wear)
Region C: Corrosion prone area (low wear, presence of cracks)
Region D: Corrosion prone area (low wear, cracks initiation)

Fig. 11. Schematic diagram of the tribocorrosion process showing various regions and mechanisms in the contact zone.

Please cite this article as: Mathew MT, et al. TiC_xO_y thin films for decorative applications: Tribocorrosion mechanisms and.... Tribiol Int (2008), doi:10.1016/j.triboint.2007.11.011

a significant effect on friction and wear behaviours based on the nature, shape and size of such particles. For instance, the lubrication properties of corrosion products formed at the interface may reduce the friction coefficient by decreasing the severity of the wear [19]. It is also known that the presence of wear debris will influence the corrosion potential at the contact zone [18,19]. However, in the present study the experiments were done at the E_{corr} of the steel, hence there is no likelihood of a predominant effect.

It was also observed that wear particles may stick to the alumina pin (which were clearly observed in this work on the pin head, immediately after the tests) and may result in a grooving mechanism during the film removal [29]. Further, as shown in the schematic diagram of the contact zone (Fig. 11), there are two regions (C and D) surrounded by the pin path, which are characterized by low wear. However, the cracks and pits that are initiated or formed because of the corrosion in the above regions, further lead to delamination of the films by layers, and also to severe wear due to the sudden sliding action of the pin (in regions A and B). It is also interesting to observe from SEM images, in the case of films with $f_O = 0.67$ (Fig. 3(c)), the presence of a special region on the surface of the film near the boundary. It is clear that such a region may result in high wear volume loss, by the synergetic effect of wear and corrosion as stated above. Moreover, the irregularities in the boundaries of the worn surface (Figs. 3(d)–(f)) testify the existence of such mechanisms in all the films, considered in the test.

3.9. Influence of film structure on tribocorrosion behaviour

As stated above (in the case of corrosion, pitting corrosion behaviour and EIS analysis, Sections 3.2 and 3.4), the study unambiguously shows that the wear–corrosion volume loss of the films is not directly influenced by their hardness or thickness, which might be again a clear sign of the strong influence of the structure of films in such situations. The XRD analysis of the various films also clarifies the above role by demonstrating its diverse structural properties. In fact, as already mentioned, the structure of films can be divided into two main zones, with an intermediate or transition zone, depending on the particular composition of the films, especially that of oxygen [17]. Zone 1 was found to be that corresponding to the lower values of oxygen (oxygen flows below approximately 2.5 sccm), which resulted in films that were identified as developing a fcc phase structure that could be a mixture of TiC and TiO. In the transition zone the films were characterized as being of a quasi-amorphous-type. Finally, in zone 2, the films were characterized by a mixed poorly crystallized rutile and anatase TiO_2 phase, corresponding to the films that were deposited with the highest oxygen amounts (corresponding to oxygen flows above approximately 4.5 sccm) [17].

Zhang and Li [34] have also pointed out in their studies on the tribological behaviour of tungsten coatings, that microstructure has a strong influence on wear performance, and suggested that fine closely packed structure shows good performance due to its superior elastic behaviour and high hardness. In turn, it is well known that the microstructure of the film is a function of film deposition parameters, substrate temperature and surface conditions, etc. [35,36]. Thus, even though the wear–corrosion volume loss agrees with above structural evaluation, as mentioned earlier, there is a need of detailed analysis for further clarification on individual film and also by considering other parameters of films, such as thickness or hardness, etc. are constant.

3.10. Limitation and scope

As it is mentioned earlier, there is a need of additional studies to clarify and understand further on the conclusions drawn from the current work. Further, the complexity created in the analysis by the presence of many parameters, which are directly/indirectly affecting the characteristics of the films is also a drawback in the study. Moreover, the electrochemical potential used in the tribocorrosion tests has been fixed as the E_{corr} of the substrate material, in order to study the basic behaviour of the films, by preventing the sudden dissolution effect of substrate material, M2 steel. However, this is not the case in real situations.

Hence, the current investigation can be extended to analyse the tribocorrosion behaviour of the films at various potentials, above E_{corr} of the substrate material or at the E_{corr} of individual films. Such analysis will assist in understanding the individual contributions from wear and corrosion and their synergistic effects on the material degradation. Also, such films have multifunctional characteristics; there is a need of further studies based on specific applications/requirements.

4. Conclusions

The following conclusions can be derived from this study:

- The study shows that all the films are protecting the steel substrate and having good performance when compared with other films considered in previous work (ZrO_xN_y films).
- It was found that the corrosion behaviour of TiC_xO_y films is more related to the film's structural features than with the basic film characteristics, such as thickness and/or number of defects (bound to the limitation of the current study). The EIS measurements also agree with the observed behaviour.
- Among all the studied samples, five of them did not show complete removal of the film. Hence, they have good tribocorrosion resistance, especially the films with $f_O = 0.55$ and 0.79.
- The mechanisms of the wear–corrosion process have been analysed, and it was observed that they might be

Please cite this article as: Mathew MT, et al. TiC_xO_y thin films for decorative applications: Tribocorrosion mechanisms and.... Tribiol Int (2008), doi:10.1016/j.triboint.2007.11.011

influenced by the wear particles and corrosion products at the contact zone.

- The contribution of wear and corrosion and their synergistic effect on the tribocorrosion process were analysed. It was observed that tribocorrosion process is dominated by wear mechanisms/process.

Acknowledgements

The authors gratefully acknowledge the financial support of the Portuguese Science Foundation (FCT) by the contracts SFRH/BPD/20377/2004, SFRH/BPD/5518/2001 and SFRH/BD/27569/2006 and by the project no. PTDC/CTM/69362/2006 co-financed by European community through FEDER.

References

[1] Eerden M. Products finishing; 2003. p. 54–9.
[2] Mitterer C, Komenda-Stallmaier J, Losbichler P, Schmolz P, Werner WSM, Stori H. Vacuum 1995;46:11.
[3] Budke E, Krempel-Hesse J, Maidof H, Schusler H. Surf Coat Technol 1999;112:108–13.
[4] Rocha LA, Ariza E, Ferreira J, Vaz F, Ribeiro E, Rebouta L, et al. Surf Coat Technol 2004;180&181:158–63.
[5] Fonseca C, Vaz F, Barbosa MA. Corros Sci 2004;46:3005–18.
[6] Gu J-D, Chen P-L. Surf Coat Technol 2006;200:3341–6.
[7] Mitterer C, Ott HM, Komenda-Stallmaier J, Schmolz P, Werner WSM, Stori H. J Alloys Compds 1996;239:183–92.
[8] Vaz F, Cerqueira P, Rebouta L, Nascimento SMC, Alves E, Goudeau Ph, et al. Surf Coat Technol 2003;174&175:197–2003.
[9] Kelly PJ, Arnell RD. Vacuum 2000;56:159–72.
[10] Toth EL. Transition metal carbides and nitrides. New York: Academic Press; 1971.
[11] Zaoui A, Kacimi S, Bouhafs B, Roula A. Physica B 2005;358:63.
[12] Dimigen H, Klages CP. Surf Coat Technol 1991;49:543.
[13] Monaghan D, Teer D, Logan P, Efeoglu I, Arnell R. Surf Coat Technol 1993;60:525.
[14] Ferreira SC, Ariza E, Rocha LA, Gomes JR, Carvalho P, Vaz F, et al. Surf Coat Technol 2006;200:6634–9.
[15] Ariza E, Rocha LA, Vaz F, Cunha L, Ferreira SC, Carvalho P, et al. Thin Solid Films 2004;469&470:274–81.
[16] European Standard EN 1811:1998. Reference test method for release of nickel from products intended to come into direct and prolonged contact with the skin.
[17] Fernandes AC, Carvalho P, Vaz F, Lanceros-Méndez S, Machado AV, Parreira NMG, et al. Thin Solid Films 2006;515:866.
[18] Jemmely P, Mischeler S, Landolt D. Tribol Int 1999;32:295–303.
[19] Pontiaux P, Wenger F, Drees D, Celis JP. Wear 2004;256:459–68.
[20] Scully JR. Corrosion 2000;56:199–218.
[21] Archard JF. Contact and rubbing of flat surfaces. J Appl Phys 1953;24:981.
[22] Yue Z, Zhou P, Shi J, Luedema KC, editors. Proceedings of the conference on wear of materials. New York: ASME; 1987. p. 763–8.
[23] Stack MM, Zhou S, Newman RC. Mater Sci Technol 1996;12:261–8.
[24] Stack MM, Pungwiwat N. Wear 2004;256(5):565–76.
[25] Stack MM, Chi K. Wear 2003;255:456–65.
[26] Ziomek-Moroz M, Miller A, Hawk J, Cadien K, Li DY. Wear 2003;255:869–74.
[27] Godet M, Berthier Y, Lancaster J. Wear 1991; p. 149–325.
[28] Williams JA, Hyncica AM. J Phys D: Appl Phys 1992;25:A81–90.
[29] Axen N, Jacobson S, Hogmark S. Tribol Int 1994;27(4):233–41.
[30] Guiemany JM, Miguel JM, Vizcaino S, Climent F. Surf Coat Technol 2001;140:141–6.
[31] Hirst W, Lancaster JK. J Appl Phys 1956;27:1057–65.
[32] Haworth RDJ. The abrasion resistance of metals. Trans ASME 1949;41:819–69.
[33] Umeda A, Sugimura J, Yamamoto Y. Wear 1998;216:22–228.
[34] Zhang H, Li DY. Wear 2003;255:924–32.
[35] Wu P-Q, Celis JP. Wear 2004;256:480–90.
[36] Sasaki M, Nakamura I, Takano I, Sawada Y. Electr. Eng. Jpn 2004;149(3):1–7.

Please cite this article as: Mathew MT, et al. TiC_xO_y thin films for decorative applications: Tribocorrosion mechanisms and.... Tribiol Int (2008), doi:10.1016/j.triboint.2007.11.011